



BNL-112085-2016-JA

***Layer-dependent quantum cooperation of electron
and hole states in the anomalous semimetal WTe₂***

**Pranab Kumar Das, D. Di Sante, I. Vobornik, J. Fujii, T. Okuda,
E. Bruyer, A. Gyenis, B. E. Feldman, J. Tao, R. Ciancio, G. Rossi,
M. N. Ali, S. Picozzi, A. Yadzani, G. Panaccione, and R. J. Cava**

Submitted to NATURE COMMUNICATIONS

February 2016

Condensed Matter Physics And Material Sciences Department

Brookhaven National Laboratory

**U.S. Department of Energy
USDOE Office of Science (SC),
Basic Energy Sciences (BES) (SC-22)**

Notice: This manuscript has been authored by employees of Brookhaven Science Associates, LLC under Contract No. DE-SC0012704 with the U.S. Department of Energy. The publisher by accepting the manuscript for publication acknowledges that the United States Government retains a non-exclusive, paid-up, irrevocable, world-wide license to publish or reproduce the published form of this manuscript, or allow others to do so, for United States Government purposes.

DISCLAIMER

This report was prepared as an account of work sponsored by an agency of the United States Government. Neither the United States Government nor any agency thereof, nor any of their employees, nor any of their contractors, subcontractors, or their employees, makes any warranty, express or implied, or assumes any legal liability or responsibility for the accuracy, completeness, or any third party's use or the results of such use of any information, apparatus, product, or process disclosed, or represents that its use would not infringe privately owned rights. Reference herein to any specific commercial product, process, or service by trade name, trademark, manufacturer, or otherwise, does not necessarily constitute or imply its endorsement, recommendation, or favoring by the United States Government or any agency thereof or its contractors or subcontractors. The views and opinions of authors expressed herein do not necessarily state or reflect those of the United States Government or any agency thereof.

Layer-dependent quantum cooperation of electron and hole states in the anomalous semimetal WTe_2

Pranab Kumar Das^{1,2}, D. Di Sante^{3,4}, I. Vobornik¹, J. Fujii¹, T. Okuda⁵, E. Bruyer³, A. Gyenis⁶, B. E. Feldman⁶, J. Tao⁷, R. Ciancio¹, G. Rossi^{1,8}, M. N. Ali⁹, S. Picozzi³, A. Yadzani⁶, G. Panaccione^{1*} and R. J. Cava^{9*}

¹ Istituto Officina dei Materiali (IOM)-CNR, Laboratorio TASC, in Area Science Park, S.S.14, Km 163.5, I-34149 Trieste, Italy

² International Centre for Theoretical Physics (ICTP), Strada Costiera 11, I-34100 Trieste, Italy

³ Consiglio Nazionale delle Ricerche - CNR-SPIN, I-67100 L'Aquila, Italy

⁴ Department of Physical and Chemical Sciences, University of L'Aquila, Via Vetoio I-67100, L'Aquila, Italy

⁵ Hiroshima Synchrotron Radiation Center (HSRC), Hiroshima University, 2-313 Kagamiyama, Higashi-Hiroshima 739-0046, Japan

⁶ Joseph Henry Laboratories and Department of Physics, Princeton University, Princeton, NJ 08544, USA.

⁷ Department of Condensed Matter Physics and Materials Science, Brookhaven National Laboratory, Upton, New York 11973, USA.

⁸ Dipartimento di Fisica, Università di Milano, Via Celoria 16, I-20133 Milano - Italy

⁹ Department of Chemistry, Princeton University, Princeton, NJ 08544, USA.

email: rcava@Princeton.EDU

*These authors contributed equally to this work

The behavior of electrons and holes in a crystal lattice is a fundamental quantum phenomenon, accounting for a rich variety of properties in solids. Boosted by the remarkable electronic and physical properties of two-dimensional (2D) materials such as graphene and topological insulators, transition metal dichalcogenides (TMDs), long of interest in materials science, have recently received renewed attention in this context. Among TMDs, the anomalous bulk properties of semimetallic WTe_2 have attracted considerable interest [1]. Here we report angle and spin-resolved photoemission spectroscopy of WTe_2 single crystals, through which we are able to disentangle the role of W and Te atoms in the formation of the band structure and to identify the interplay of the charge, spin and orbital degrees of freedom. Supported by first-principles calculations and high-resolution surface topography, we reveal the existence of a layer-dependent electronic behavior. The balance of electron and hole states is found only when considering at least three Te-W-Te layers, showing that the behavior of WTe_2 is in between those expected for 2D and 3D electronic systems. The observed evolution as a function of depth from the surface indicates that WTe_2 provides an excellent platform to study the effect of dimensionality on the quantum properties of matter.

TMDs are a group of layered materials with chemical formula MX_2 , where M is a transition metal and X can be S, Se, or Te. Their properties span from pure insulators to good metals, and they also exhibit various low temperature phenomena such as metal-insulator transitions, superconductivity and charge density waves [2]. An important aspect of TMDs is the presence of anisotropic bonding with different strengths: the X-M-X building blocks are stacked along the crystallographic c-direction, and while the inter-layer interaction is mainly of weak van der Waals type, the intra-layer bonding between the atoms is strong and covalent. Dimensionality

is thus expected to play a significant role in TMDs, because the transition from a single or a few layers to bulk implies significant change in the symmetry of the orbitals and in quantum confinement, producing important differences in the electronic structure.

Among TMDs, WTe_2 is special because it displays an additional structural distortion: the tungsten atoms form zigzag chains along the crystallographic a -axis, producing a quasi 1D arrangement. Moreover, WTe_2 is a semimetal with a reduced density of states at the Fermi level coming from small overlap between valence and conduction bands without a band gap. It exhibits an extremely large uniaxial positive magnetoresistance with no saturation up to a magnetic field as high as 60 T [1], which has been attributed to perfect electron and hole compensation. In addition, the presence of two heavy elements points to the importance of spin orbit coupling (SOC) in determining the details of the Fermi surface and/or the relevant low energy excitations of the system.

Here, by combining results of scanning tunneling microscopy (STM), spin and angle-resolved photoemission spectroscopy (ARPES), and layer-resolved ab-initio calculations, we explored the details and the evolution of electron and hole states in WTe_2 . Our data reveal significant differences between surface and bulk electronic properties, with a clear evolution as a function of depth from the surface. The Fermi surface measured by ARPES is significantly reduced with respect to the one calculated for the bulk, indicating the presence of a reduced, yet still balanced, number of electrons and holes at the surface and near-surface region. The importance of SOC is directly shown by spin resolved ARPES measurements, and the data are consistent with our theoretical calculations.

To visualize the surface quality of WTe_2 , we performed high resolution scanning tunneling microscopy (Fig. 1). The STM images reveal that the top layer is composed of two inequivalent Te atoms, labeled Te1 and Te2 in Fig. 1b (see also supplementary information). The surface is atomically ordered with extremely high quality and low impurity concentration, with approximately 1 underlying defect per 3000 atoms observed (Fig. 1a), corresponding to $\approx 9 \times 10^{11}$ defects/cm². In addition, the topographic image and its Fourier transform (Fig. 1c) clearly show that the electronic structure of the surface has an angular distortion, similar to that reported previously [3, 4]. We observe the distortion at multiple tip-sample biases, in multiple samples, and with different STM tips, indicating that this finding is not related to thermal drift, tip artifacts, or a particular energy (see supplementary information). Comparison with TEM data suggests that the distortion is due to surface reconstruction and model calculations for a single WTe_2 monolayer show that it does not significantly affect the band structure (see supplementary information).

We next explore the detailed electronic structure of WTe_2 and the related layer dependence of the electron and hole states. In Figure 2b we show the experimental E vs. k ARPES spectra overlaid with bulk theoretical band structures calculated using density functional theory (DFT) with (red bands on the left) and without (blue bands on the right) SOC, along the reciprocal space line ΓX . Following the standard procedure and assuming WTe_2 as a pure 2D layered system, calculations are performed with out-of-plane k-vector component $k_z=0$. We observe well-defined electron and hole pockets at the Fermi energy along the tungsten chain direction (ΓX), confirming previous results [5]. However, a detailed comparison of the observations to bulk theoretical band structure as described above presents some inconsistencies. The

theoretical position of the electron pocket is significantly further away from the zone center and its maximum binding energy is larger than the measured one by more than a factor two. The presence of heavy atoms like W and Te suggests that SOC plays an important role in the interpretation of WTe_2 spectral features. The changes in the theoretical band structure associated with SOC (Fig.2b, red curves) illustrate that relativistic effects cannot be neglected in WTe_2 , and although we obtain somewhat better results, a quantitative agreement is not found in either case. We also note a non-negligible k_z band dispersion [1, 5] when comparing experimental spectra with theoretical bands for reciprocal lines parallel to ΓX at different k_z momenta, ranging from the Brillouin zone center ($k_z=0$) to the Brillouin zone edge ($k_z=\pi/c$) (see supplementary information). However, including k_z dispersion does not result in an improved agreement between calculation and experiment.

We find a significant improvement, however, when using a more realistic model that takes into account the contribution of individual layers. This model is based on a supercell made by van der Waals-bonded WTe_2 planes stacked along the [001] direction (Fig. 2a). From the large number of bands in the supercell calculations, we are able to isolate the individual contribution of each WTe_2 plane in the stack by projecting the electronic band structure onto the atoms belonging to that given plane only. We note that the experimental ARPES spectra correspond to a weighted spectral intensity from the different layers probed, and the contributions of deeper layers are exponentially attenuated by the inelastic mean free path of photoelectrons. Superimposing the theoretical bands on the experimental spectra, and projecting onto the first, second and third WTe_2 planes (Figs. 2c-e, respectively), we filter the layer-dependent information about the electronic structure because we are able to correlate individual features

of the layer-resolved calculations in the experimental spectra. In this analysis, the size of the plotted circles is proportional to the contribution of the given WTe_2 plane: the bigger the circle, the larger the contribution of that plane to the spectral features. We thus observe in Fig. 2c that the electron pocket is located at 0.35 \AA^{-1} from the zone center (highlighted by the blue arrow) and is present even when only the first Te-W-Te layer is considered. The hole pocket (blue arrow in panel e) starts appearing only when taking into account the presence of the third layer, and thus has a more bulk-like character. Furthermore, we cannot exclude the existence of a small hole pocket at Γ , as recently proposed by theoretical findings [6] for an isolated WTe_2 monolayer (note that in the same work the electron pockets are closer to the zone center, similar to our case); a similar hole pocket has also recently been observed in other ARPES experiments [7]. In our case (Fig. 2), the hole pocket is fully occupied, and the range of explored temperatures is well below the Lifshitz transition recently reported at above 160 K [8]. Given that the hole pocket is very close to E_F , the difference could be due to temperature induced shift of the chemical potential as proposed in ref. [8]. Moreover, hole pockets close to each other on either side of the Γ point would justify the unusual magnetic breakdown observed in quantum oscillations [9].

We further stress that our slab calculations do not reveal the existence of distinct surface states. This is supported by the comparison of bulk theoretical band structures for different k_z momenta with the electronic states of the slab (see supplementary information). In fact, all bulk bands lie within the continuum of the slab's bulk band structure projected onto the surface Brillouin zone. Indeed, the bands shown in Fig. 2c-e overlaid to ARPES spectra are bulk states showing substantial spectral weight on the topmost surface layers; this seems in analogy to

what is observed in MoS₂ and many other systems, like iron pnictides, with cleaved neutral surfaces [10, 11].

The present analysis not only provides a quantitative agreement between experiment and theory in terms of dispersion and momentum space locations of electronic states, but clearly shows the presence of a layer-dependent evolution of electron and hole states: a bulk-like electronic structure, characterized by the electron-hole charge balance is obtained only when more than two Te-W-Te layers are taken into account. Our results clearly display some analogies with other ‘less than 3D’ materials: in the case of topological insulators for example it has been theoretically predicted and experimentally confirmed not only that the critical thickness of six quintuple layers is needed to set the topological properties of the surface but also that the spin-orbital texture of a topological insulator evolves in a layer-dependent manner, extending over several nanometers from the surface [12,13].

Given that a nearly equal concentration of electrons and holes is a necessary condition for non-saturating magnetoresistance to be observed in two-component systems [14, 15], the present observation has important implications towards the realization of devices based on few-layer TMDs [16].

To further check the robustness and the reliability of our theoretical interpretation, we used two different approaches: i) an ab-initio tight-binding model for a 40 layers slab (thickness about 42 nm, see supplementary information); ii) a renormalization scheme for semi-infinite systems to calculate the surface spectral function, shown in Fig. 2f [17] (see Methods for details). These checks aimed at excluding spurious effects arising from the interaction between

the two extreme surfaces (always present in slab calculations if the number of layers is not large enough). The theoretical bands of Fig. 2f provide a direct link with the measured E vs. k intensity maps (except for dipole matrix elements, neglected in our calculations). By using both methods, most of the experimental features are well reproduced, in particular the hole and electron pockets near E_F as well as the bands at higher binding energy. Moreover, no remarkable differences are observed in comparison with the DFT results for the six-layers-thick slab.

Figure 3 shows the experimental (left panel) and bulk theoretical (right panel) constant energy cuts from E_F down to 100 meV binding energy, in steps of 20 meV. The theoretical results qualitatively reproduce the main features of the Fermi surface, including the shape and the distribution of the pockets and a finite intensity at Γ (i.e. confirming the presence of a possible hole pocket at Γ). However, the calculated bulk features have a significantly larger area than the measured Fermi surface, providing further evidence that simply recasting bulk calculations is insufficient to explain the experimentally observed ARPES features. The area of the Fermi surface calculated by the bulk theoretical model is larger than the area of the observed Fermi surface, which implies that the total number of carriers is larger in the bulk than on the surface. In spite of this difference, the comparison shows that the balance between electrons and holes is maintained in both cases, to within the sensitivity of our technique (see also Fig. S9). This in turn indicates that the balancing between electrons and holes, i.e. their ‘quantum-cooperation’ over different layers, is the dominant factor that determines the macroscopic properties of the system such as also the non-saturating magnetoresistance.

In order to determine the role of SOC and obtain insight into the spin texture, we performed spin-resolved measurements at a number of \mathbf{k} points in the Brillouin zone. Spin resolved ARPES spectra are presented in Fig. 4, as measured at the hole pocket (panels a, c; blue and yellow circles), close to Γ on the ΓX line (panel b, red circle) and close to Γ , but off the ΓX line (panel d, green circle). Panel f shows the calculated spin resolved band structure along ΓX .

We measure a sizeable spin polarization (P) for an extended binding energy range. It reaches more than 35% for P_y at a binding energy of 0.55 eV (panel a, black arrows). This indicates that there must not only be a broken space inversion symmetry but also a significant influence of SOC in WTe_2 . The spin texture is quite complex, with large oscillations in value and sign of P in a narrow energy window, clearly visible in both P_y and P_z (Fig. 4a). This observation is confirmed by the calculation in Fig. 4f. Experimental error cannot exclude the presence of a finite spin polarization at E_F , but it is negligible with respect to those observed at higher binding energies. The fine spectral structures in the calculation are not visible in the experimental spin polarization measurements, due to the experimental energy and angular resolution. However, we obtain notable qualitative agreement, as detailed below. The P_x component is zero along the ΓX line (Figs. 4a,b), while we observe non-zero P_x component for points away from ΓX (Fig. 4d). This means that the electron spin along ΓX is perpendicular to the W chains, in agreement with calculations that predict only large P_y and P_z spin polarizations (Fig. 4f). The results shown in Figs. 4 a,b (at the hole pocket) and Fig. 4f reveal the presence of both in-plane and out-of-plane components of the spin polarization, in contrast with ordinary Rashba systems where P is only in-plane [18]. The spin polarization changes sign upon crossing the Brillouin zone center, i.e., the sign of P is reversed at $\mathbf{k}' = -\mathbf{k}$, as experimentally confirmed in Fig. 4a and 4c, which

show data taken at positive and negative k_x values. This indicates that time reversal symmetry is preserved, i.e. $[E(\mathbf{k}, \uparrow) = E(-\mathbf{k}, \downarrow)]$ and that the observed spin polarization of bands has nonmagnetic origin. A large spin polarization of electronic bands has been recently reported in the semiconducting TMD WSe_2 , where P occurs due to the local asymmetry of layers [19] (consecutive Se-W-Se layers have opposite net dipole moment, which modulate the spin texture strongly even though the global inversion symmetry is preserved in the crystal). Unlike WSe_2 , the crystal structure of WTe_2 is non-centrosymmetric. Therefore, by symmetry consideration one naturally expects a lifting of the spin degeneracy via spin-orbit coupling. The amplitude of spin polarization depends on many different factors (i.e., orbital character, band gap, electric fields etc.), but primarily on the strength of the SOC; therefore, our results indicate that SOC is clearly reflected in the spectral function of WTe_2 , as also recently reported by CD-ARPES results [7].

Considering our present results from a more general perspective, it is important to underline that exact carrier compensation is a necessary, yet not sufficient, condition for a non-saturating quadratic behavior of magnetoresistance [14]. Bismuth, provides an example where compensation is observed, but quadratic dependence of resistance in a magnetic field and non-saturation are not [14, 20]. Other prerequisites for behavior like that observed in WTe_2 are: a) low density of impurities and defects and b) a carrier density far from the quantum limit [21, 22]. Here we have shown that condition a) is nearly fulfilled as shown by STM results, and condition b) is supported by the reported low resistivity and high mobility in WTe_2 [1, 6, 23]. These observations suggest that future experiments exploring the relationship between

electronic structure and magnetoresistance in WTe_2 would be worthwhile and that WTe_2 could be a potential candidate to form an excitonic dielectric in the Abrikosov sense [21,24].

In summary, our theoretical and experimental ARPES findings provide clear evidence that the electronic properties of WTe_2 display a layer-dependent evolution from surface to bulk, i.e., it cannot be considered a-priori as a non-interacting 2D layered system, in agreement also with recent temperature-dependent magnetoresistance measurements [25]. The balance between hole and electron states, representing one of the crucial conditions for the non-saturating magnetoresistance in this system, is established only beyond finite number of layers (three) and maintained in the bulk. This consideration provides a fundamental input for future exploitation of TMDs in general, and WTe_2 in particular, in devices and heterogeneous interfaces.

References:

1. Ali M. N., Xiong J. et al. Large, non-saturating magnetoresistance in WTe_2 , *Nature* **514**, 205-208 (2014)
2. Wang Q. H., Kalantar-Zadeh K. et al, Electronics and optoelectronics of two-dimensional transition metal dichalcogenides, *Nature Nanotechnology* **7**, 699-712 (2012)
3. A. Crossley, S. Myhra, C.J. Sofield: STM analysis of WTe_2 surfaces — correlation with crystal and electronic structures - *Surface Science* **318**, 39-45 (1994)
4. S.W. Hlaa, V. Marinković, A. Prodana, I. Muševića: STM/AFM investigations of β - $MoTe_2$, α - $MoTe_2$ and WTe_2 - *Surface Science* **352-354**, 105-111 (1996)
5. Pletikosić I., Ali M. N., Fedorov, A. V. Cava R. J., Valla T., Electronic Structure Basis for the Extraordinary Magnetoresistance in WTe_2 , *Phys. Rev. Lett.* **113**, 216601 (2014)
6. Lv H. Y., Lu W. J., Shao D. F., Liu, Y., Tan S. G., Sun Y. P., Perfect charge compensation in WTe_2 for the extraordinary magnetoresistance: From bulk to monolayer, *Europhysics Letters*, **110** 37004 (2015)
7. Jiang J., Tang F. et al. Signature of strong spin-orbital coupling in the large nonsaturating magnetoresistance material WTe_2 , *Phys. Rev. Lett.* **115**, 166601 (2015)
8. Y. Wu, N.H. Jo, M. Ochi, L. Huang, D. Mou, S.L. Bud'ko, P.C. Canfield, N. Trivedi, R. Arita, A. Kaminski, Temperature induced Lifshitz transition in WTe_2 , *Phys. Rev. Lett.* **115**, 166602 (2015)

9. Zhu Z., Lin X. et al. Quantum Oscillations, Thermoelectric coefficients, and the Fermi Surface of Semimetallic WTe₂, Phys. Rev. Lett. **114**, 176601 (2015)
10. M. Gehlmann, G. Bihlmayer, I. Aguilera et al. Quasi 2D electronic states with high spin-polarization in centrosymmetric MoS₂ bulk crystals, arXiv:1510.04101, <http://arxiv.org/abs/1510.04101>
11. Alexander Lankau, Klaus Koepf, Sergey Borisenko et al. Absence of surface states for LiFeAs investigated using density functional calculations, Phys. Rev. B **82**, 184518 (2010).
12. Zhang Y., He K., Chang C., Crossover of the three-dimensional topological insulator Bi₂Se₃ to the two-dimensional limit, Nature Physics **6**, 584-588 (2010)
13. Zhu Z. H., Levy G., Rashba Spin-Splitting Control at the Surface of the Topological Insulator Bi₂Se₃, Phys. Rev. Lett. **107**, 186405 (2011)
14. Alekseev P. S., Dmitriev A. P. et al. Magnetoresistance in Two-Component Systems, Phys. Rev. Lett. **114**, 156601 (2015)
15. Parish M. M. and Littlewood P. B., Non-saturating magnetoresistance in heavily disordered semiconductors, Nature **426**, 162-165 (2003)
16. Lin Wang, Ignacio Gutiérrez-Lezama, Céline Barreateau, Nicolas Ubrig, Enrico Giannini, A.F. Morpurgo, Tuning Magnetotransport in a Compensated Semimetal at the Atomic Scale, arXiv:1510.04827, <http://arxiv.org/abs/1510.04827>
17. Henk J. and Schattke W., A subroutine package for computing Green's functions of relaxed surfaces by the renormalization method, Comput. Phys. Commun. **77**, 69-83 (1993)
18. Hasan M. Z, Kane C. L., Colloquium: Topological insulators, Rev. Mod. Phys. **82**, 3045 (2010)
19. Riley J. M., Mazzola F., et al. Direct observation of spin-polarized bulk bands in an inversion-symmetric semiconductor, Nature Physics **10**, 835-839 (2014)
20. Liang T., Gibson Q., et al. Evidence for massive bulk Dirac fermions in Pb_{1-x}Sn_xSe from Nernst and thermopower experiments, Nature Commun. **4**, 2696 (2013)
21. A.A. Abrikosov The Transformation of a Semimetal into an Exciton Dielectric in a Strong Magnetic Field, Soviet Physics Uspekhi **15**, **5**, 53 (1974)
22. E.W. Fenton, Electrical resistivity of semimetals in the extreme quantum limit, Journal of low temperature Physics **7**, vol.576, 415 (1972)
23. Ali, M.N., Schoop, L., Xiong, J., Flynn, S., Gibson, Q., Hirschberger, M., Ong, N.P., and Cava R.J., Correlation of Crystal Quality and Extreme Magnetoresistance of WTe₂, EPL **110**, 67002 (2015)
24. A.A. Abrikosov, Quantum linear magnetoresistance Europhys. Lett., **49** (**6**), pp. 789–793 (2000)
25. L. R. Thoutam, Y. L. Wang, Z. L. Xiao, S. Das, A. Luican-Mayer, R. Divan, G. W. Crabtree, and W. K. Kwok, Temperature-Dependent Three-Dimensional Anisotropy of the Magnetoresistance in WTe₂, Phys. Rev. Lett. **115**, 046602 (2015)

26. Panaccione G., Vobornik I., Fujii J. et al. Advanced Photoelectric effect experiment beamline at Elettra: A surface science laboratory coupled with Synchrotron Radiation, *Rev. Sci. Instrum.* **80**, 043105 (2009)
27. Okuda T., Miyamaoto K. et al. Efficient spin resolved spectroscopy observation machine at Hiroshima Synchrotron Radiation Center, *Rev. Sci. Instrum.* **82**, 103302 (2011)
28. Kresse G., Furthmüller J., Efficient iterative schemes for *ab initio* total-energy calculations using a plane-wave basis set, *Phys. Rev. B* **54**, 11169 (1996)
29. Kresse G., Joubert D., From ultrasoft pseudopotentials to the projector augmented-wave method, *Phys. Rev. B* **59**, 1758 (1999)
30. Mar A., Jovic S., Ibers A, Metal-metal vs tellurium-tellurium bonding in WTe_2 and its ternary variants $TaIrTe_4$ and $NbIrTe_4$, *J. Am. Chem. Soc.* **114**, 8963 (1992)
31. Grimme S., Semiempirical GGA-type density functional constructed with a long-range dispersion correction, *Comp. Chem.* **27**, 1787 (2006)
32. Mostofi A. A., Yates J.R., Lee Y.-S., Souza I., Vanderbilt D., Marzari N., *Comput. Phys. Commun.* **178**, 685 (2008)

Figure Captions

Figure 1: Surface topography and structure of WTe_2 (a) Topographic image of a $400 \text{ \AA} \times 400 \text{ \AA}$ area on the (001) surface of WTe_2 with several ‘tie-fighter’-like impurities ($V_{\text{bias}} = -80 \text{ mV}$, $I_{\text{tunneling}} = 100 \text{ pA}$ and $T = 30 \text{ K}$). Inset: Zoom-in on an individual defect. (b) Side schematic view of the WTe_2 lattice highlighting the two inequivalent Te atoms. (c) Fourier transform of the topograph in (a) reveals Bragg peaks corresponding to the atomic corrugation (red circles indicate the first order Bragg peaks) and the anomalous angle between the crystallographic axes on the surface (6° in this sample). The degree of the angular distortion varied a few degrees between different samples. (d) Zoom-in on a clean area displays the surface Te atoms. (e) Top schematic view of the WTe_2 (001) surface highlighting the surface Te atoms and the unit cell dimensions.

Figure 2: Evolution of band structure with number of layers. a) Crystal structure of WTe_2 with the bulk and surface Brillouin zones on the right. On the left, the slab model used in the theoretical calculations, consisting of 6 Te-W-Te layers; each layer is formed by hexagonally packed W sandwiched between two Te layers. b-e) ARPES measurements ($h\nu = 68$ eV, $T = 77$ K) of the electronic structure along the ΓX high symmetry direction (along the W chains). b), bulk electronic structures as calculated with SOC (red bands at negative momenta) and without SOC (blue bands at positive momenta); c) theoretical bands projected on the topmost WTe_2 planes d,e) theoretical bands projected on second and third plane, respectively. In panels c) and e) blue arrows mark the positions of the theoretical electron and hole pockets, respectively. In panels b) to e) the size of the circles is proportional to the weight of the layer-resolved orbital character, calculated as the sum of the orbital characters of all the atoms belonging to the respective layer. Panel f): the theoretical surface spectral function $A(\mathbf{k}, E)$.

Figure 3: Fermi surface topography. Constant energy cuts from E_F down to 100 meV binding energy (in steps of 20 meV). Left: experimental spectra measured at a photon energy of 68 eV and at 77 K, right: theoretical calculations for bulk WTe_2 .

Figure 4: Experimental and theoretical spin polarized band structure of large SOC and non-centro-symmetric WTe_2 . a)-d) measured spin resolved ARPES spectra (red and blue curves) and spin polarization (green curves) at four distinct \mathbf{k} points as indicated in panel e); e) experimental Fermi surface with the corresponding spin measurement positions; f) calculated band structure along k_x direction, upper/lower panel shows S_y/S_z spin orientation; g) experimental geometry of spin resolved ARPES setup. In panel a) (S_y), the down spin spectrum (red curve) has a larger

peak at 0.6 eV (down arrow) and the up spin spectrum (blue curve) has a larger peak at 0.2 eV (up arrow), while at panel c), on the contrary, the up spin spectrum has a dominating peak at 0.6 eV and the down spin spectrum has a dominating peak at 0.2 eV, supporting time reversal effect.

Methods

ARPES. ARPES experiments were performed at APE-IOM beamline [26] at the ELETTRA Sincrotrone Trieste. High quality surfaces were obtained by cleaving the samples in UHV at a base pressure of 1×10^{-10} mbar. The crystallographic orientation was examined by low energy electron diffraction (LEED) patterns. Core levels, valence-band, and Fermi surface measurements were performed using a high resolution VG-SCIENTA DA30 electron analyzer, in a photon energy range of 20–100 eV, with an angular and energy resolution better than 0.2 deg and 20 meV, respectively. The low temperature data are collected at 16 K using a liquid helium cooled cryostat. **STM.** Prior to the measurements, the samples were cleaved in ultra-high vacuum at room temperature and immediately transferred to our home-built variable temperature STM. Measurements were performed at 28 K. **Spin-Resolved ARPES.** Spin resolved ARPES experiments were performed at HiSOR [27]. The spin resolved spectra were measured by means of VLEED spin detector using Fe-O target; two VLEED detectors positioned orthogonally are able to measure the x, y (in-plane) and z (out of plane) components of the spin polarization. Standard *He* laboratory light source ($h\nu = 21.22$ eV) was used as incident beam at various temperatures down to 10 K. The asymmetry of the spin polarization was quantified by reversing the current through a coil. The analyzer resolution of SR-ARPES was 60 meV and

the angular resolution was 1.5 deg. The spin asymmetry A is given by $A = (I_+ - I_-)/(I_+ + I_-)$. The actual polarization P depends on the instrument and detector setup (target), and is given by $P = A/S_{\text{eff}}$, where S_{eff} is the effective Sherman function value corresponding to the detector and instrumental setup used. Here we have used $S_{\text{eff}} = 0.2$. Next the up and down spin component $S_{\uparrow}, S_{\downarrow}$ can be calculated following the expression $S_{\uparrow}(S_{\downarrow}) = (1 \pm P)(I_+ + I_-)/2$.

Density Functional Theory Calculations. Supercell calculations were performed using the generalized gradient approximation (GGA) as implemented in the DFT code Vienna Ab-Initio Simulation Package (VASP) [28, 29]. Atomic positions were fully relaxed starting from data in Ref. [30]. We used the projector augmented wave (PAW) method by explicitly treating 6 valence electrons both for W and Te, while d electrons of Te were kept within the core of the PBE pseudopotentials. Integration over the first Brillouin zone was made with a 12x8x1 Monkhorst-Pack k-mesh centered at Γ (24x12x2 for bulk calculations). For all the simulations, a 400 eV plane-wave energy cutoff was used. Spin-orbit coupling has been self-consistently taken into account. Dipole corrections, as implemented in VASP, were applied along the z direction in order to counteract any spurious electric field that might arise from periodic boundary conditions in the presence of a dipole moment normal to the surface in a slab geometry (with 20 Å-thick layer of vacuum). To model surface as well as more bulk features, we considered a slab containing 6 planes of WTe_2 stacked onto each other along the [001] direction. The effects of van der Waals interactions between WTe_2 planes has been properly taken into account by the DFT-D2 method of Grimme [31], but no significant differences in the electronic properties have been detected with respect to GGA calculations.

In order to calculate bulk Fermi surfaces reported in Fig 3 (right panel), we adopt a two step procedure: i) firstly, we projected the bulk Hamiltonian onto a basis made of W s and d, and Te s and p orbitals, for a total of 112 Wannier functions, by means of the WANNIER90 package [32]; ii) subsequently, the Wannier Hamiltonian is used to build up the bulk Green's function as $G(\mathbf{k},w)=1/(w-H(\mathbf{k})+i\delta)$, which in turns gives the Fermi surface maps at the chosen binding energy w . Theoretical spectral functions have been calculated within the framework of the surface renormalization method [17] based on the same Wannier Hamiltonian as described before. The surface spectral function is defined as $A(\mathbf{k},w)=-(1/\pi)\text{Im}G_{\text{surf}}(\mathbf{k},w)$, where $G_{\text{surf}}(\mathbf{k},w)$ represents the angular and energy resolved surface Green's function. Major differences between $A(\mathbf{k},w)$ and ARPES data, as for example line intensities and high- \mathbf{k} features, possibly rely in the absence of transition matrix elements in the theoretical description.

Acknowledgements

This work has been partly performed in the framework of the nanoscience foundry and fine analysis (NFFA-MIUR Italy) project. The electron diffraction study at Brookhaven National Laboratory was supported by the DOE BES, by the Materials Sciences and Engineering Division under contract DE-AC02-98CH10886, and through the use of the Center for Functional Nanomaterials. The work at Princeton was supported by the National Science Foundation MRSEC program grant DMR-1420541, with STM support from NSF-DMR-1104612, ARO-W911NF-1-0262, ARO-MURI program W911NF-12-1-0461, and DARPA-SPWAR Meso program N6601-11-1-4110. D. di S. and S. P. acknowledge the CARIPO Foundation through the MAGISTER project Rif. 2013-0726. This work was partly supported by the Italian Ministry of Research through the project PRIN Interfacce di ossidi: nuove propriet  emergenti, multifunzionalita` e dispositivi per elettronica e energia (OXIDE).

Author contributions

R. J. C. and G.P. conceived the experiment and wrote the paper with contributions from D. di S. and I.V. All authors discussed the results, commented manuscript and prepared written contributions. R.J.C. and M.N.A. grew the crystals and characterized samples. J.T. performed the electron diffraction experiments. A.G, B.E.F. and A. Y. performed STM experiments and analysis. D. di S., E. B. and S. P. performed calculations. P.K.D., I.V., G.P., G.R., J.F, R.C., and T.O. performed synchrotron radiation experiments and analyzed the data.

Additional information

Correspondence and requests should be addressed to R.J.C.

Competing financial interests

The authors declare that they have no competing financial interests.

Figure 1

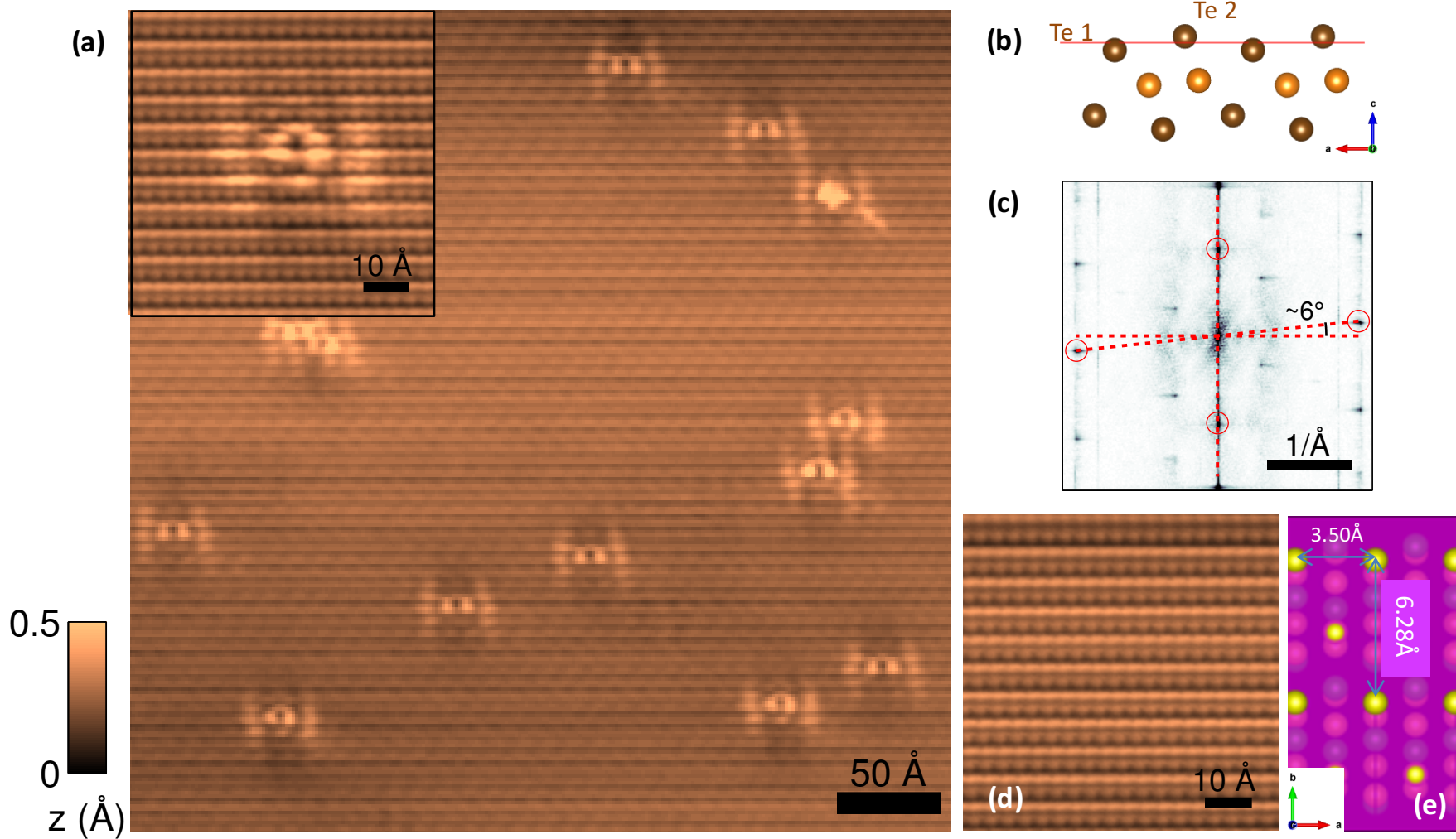


Figure 2

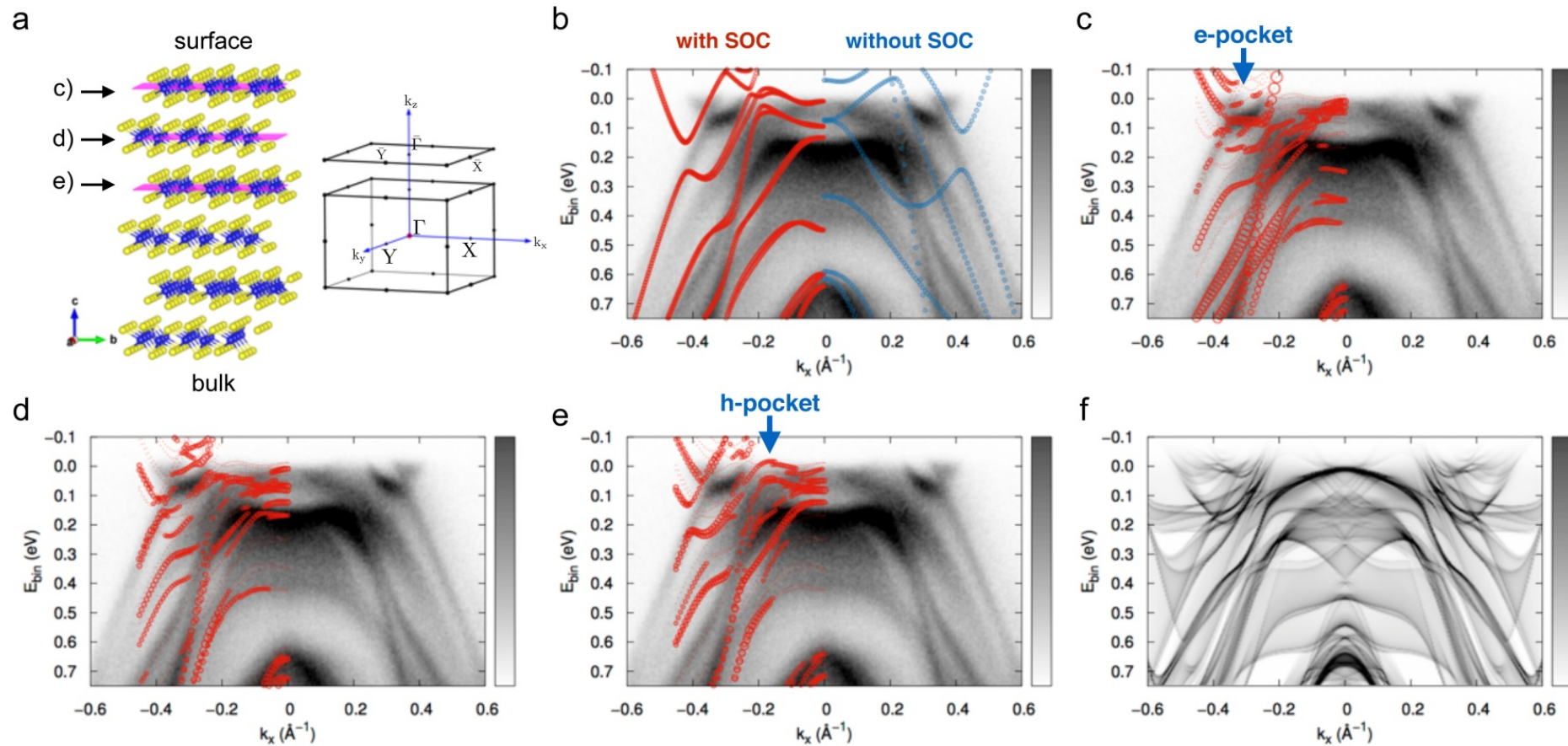


Figure 3

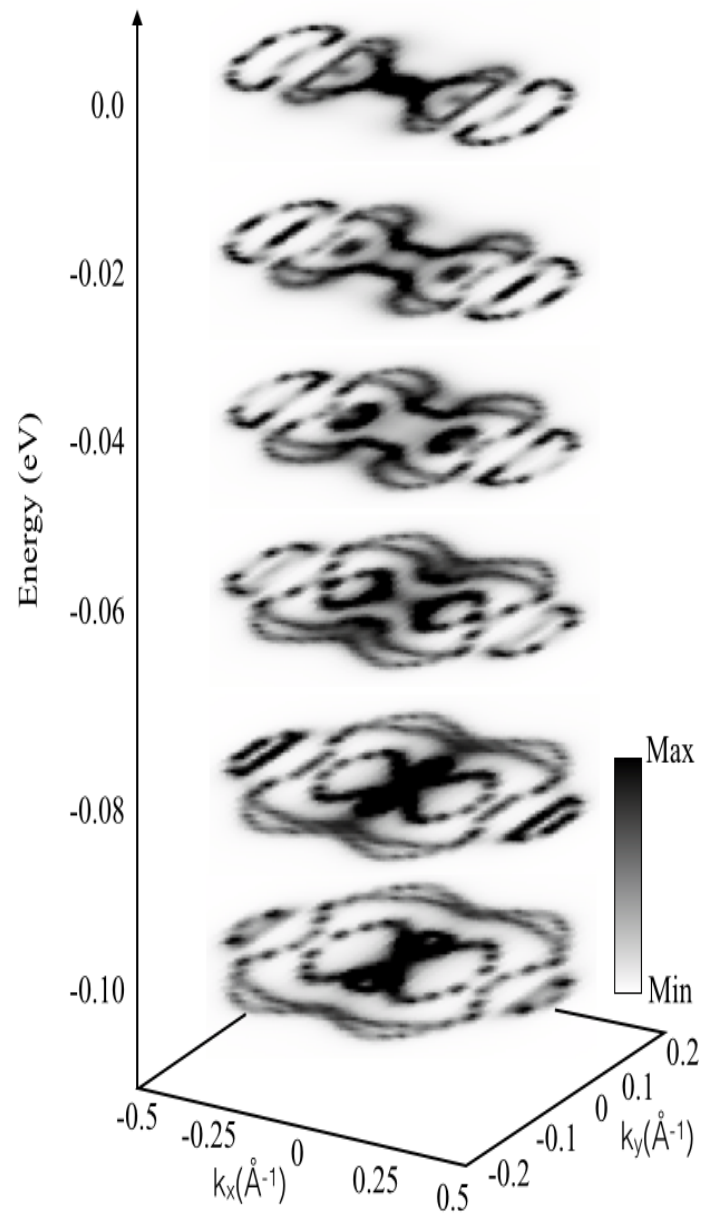
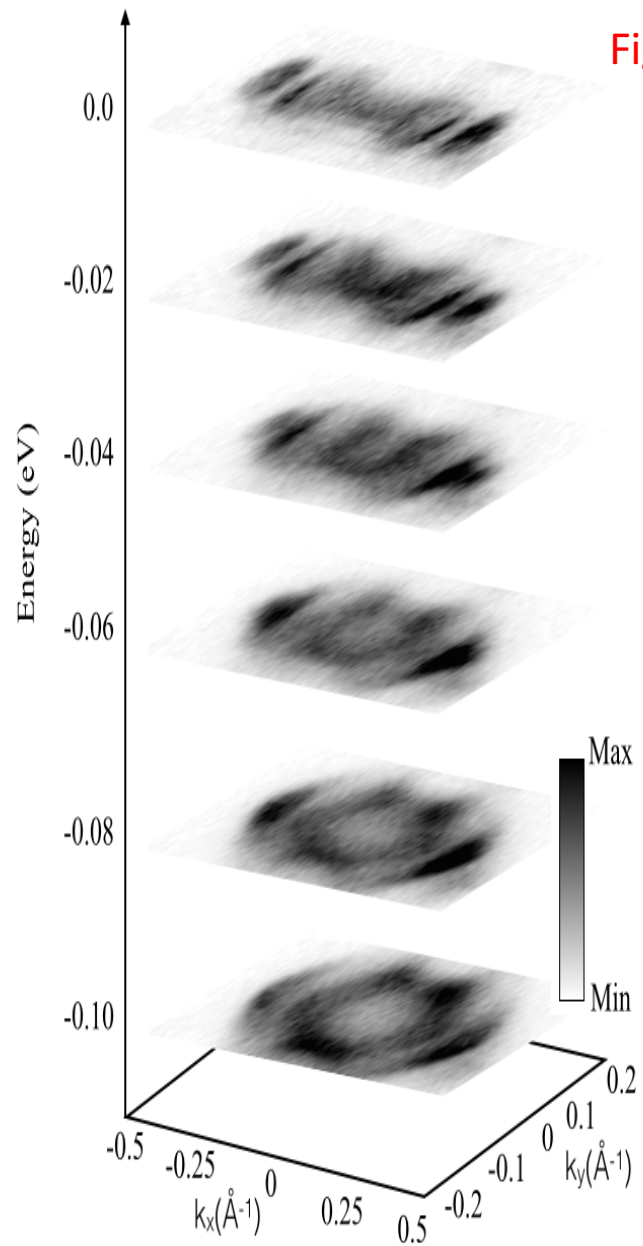
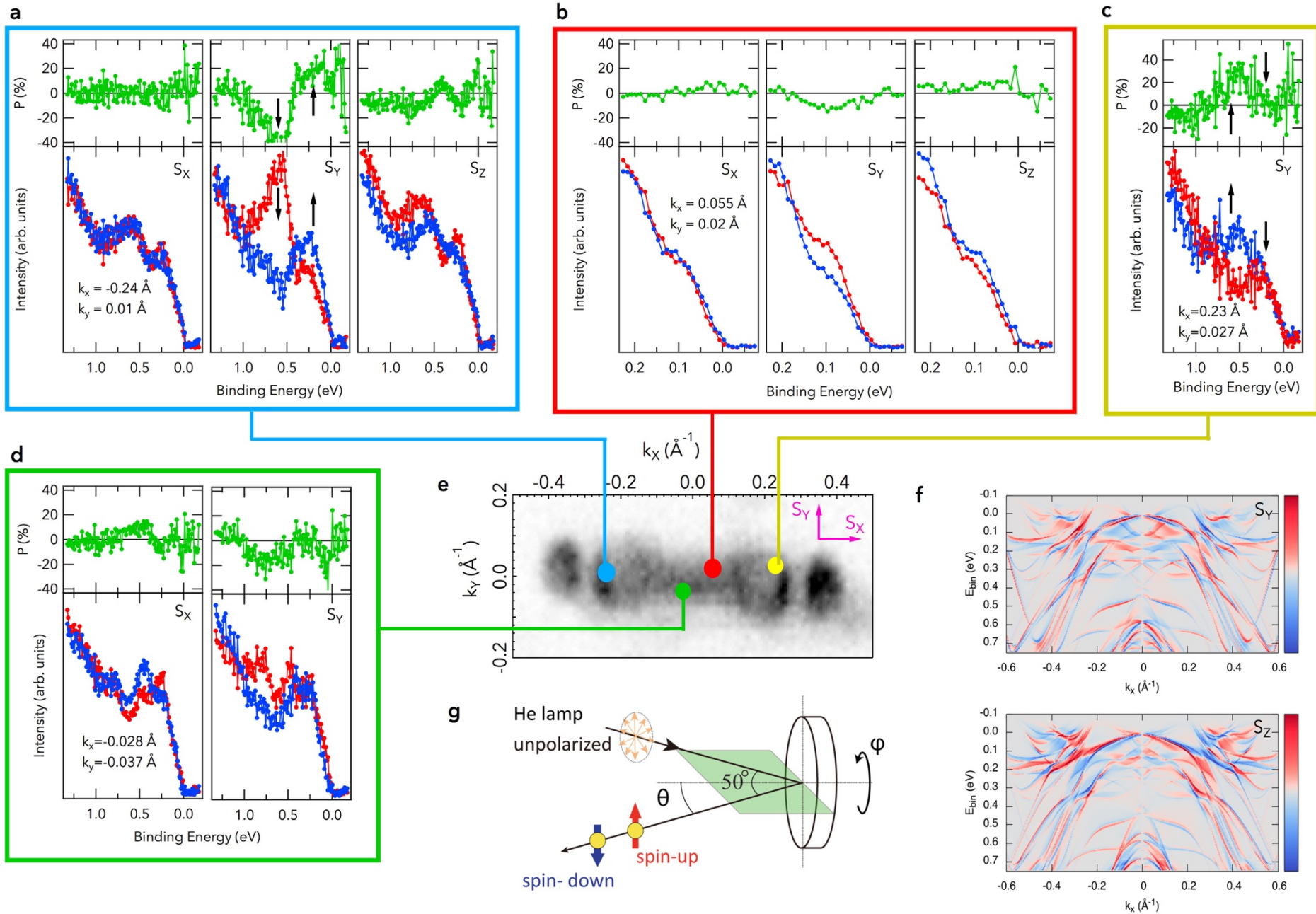


Figure 4



SUPPLEMENTARY INFORMATION

Layer-dependent quantum cooperation of electron and hole states in the anomalous semimetal WTe_2

Pranab Kumar Das^{1,2}, D. Di Sante^{3,4}, I. Vobornik¹, J. Fujii¹, T. Okuda⁵, E. Bruyer³, A. Gyenis⁶, B. E. Feldman⁶, J. Tao⁷, R. Ciancio¹, G. Rossi^{1,8}, M. N. Ali⁹, S. Picozzi³, A. Yadzani⁶, G. Panaccione^{1*} and R. J. Cava^{9*}

¹ Istituto Officina dei Materiali (IOM)-CNR, Laboratorio TASC, in Area Science Park, S.S.14, Km 163.5, I-34149 Trieste, Italy

² International Centre for Theoretical Physics (ICTP), Strada Costiera 11, I-34100 Trieste, Italy

³ Consiglio Nazionale delle Ricerche - CNR-SPIN, I-67100 L'Aquila, Italy

⁴ Department of Physical and Chemical Sciences, University of L'Aquila, Via Vetoio I-67100, L'Aquila, Italy

⁵ Hiroshima Synchrotron Radiation Center (HSRC), Hiroshima University, 2-313 Kagamiyama, Higashi-Hiroshima 739-0046, Japan

⁶ Joseph Henry Laboratories and Department of Physics, Princeton University, Princeton, NJ 08544, USA.

⁷ Department of Condensed Matter Physics and Materials Science, Brookhaven National Laboratory, Upton, New York 11973, USA.

⁸ Dipartimento di Fisica, Università di Milano, Via Celoria 16, I-20133 Milano - Italy

⁹ Department of Chemistry, Princeton University, Princeton, NJ 08544, USA.

email: rcava@Princeton.EDU; panaccione@elettra.eu

*These authors contributed equally to this work

1. Surface distortion

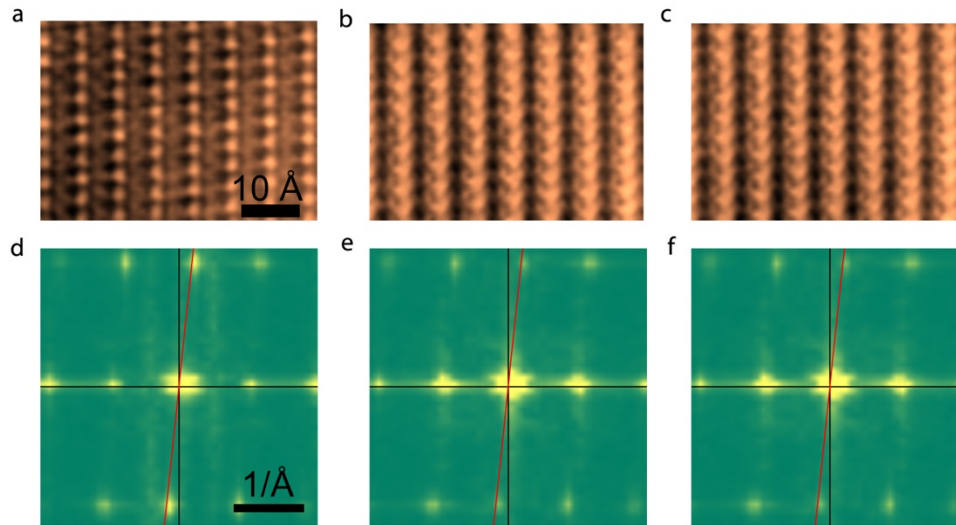


Figure S1: Panel a-c: Topographic images of the (001) surface of WTe₂ acquired at different bias voltages of 200 mV, 100 mV, -100 mV, respectively, and corresponding Fourier transforms of the topographs (panel d-f), where the surface distortion between the crystallographic axes is found (6° in this sample, independent of tip-sample bias). The degree of the angular distortion varied a few degrees between different samples.

Fig. S1 shows topographic images at different bias voltages and corresponding Fourier-transform of a representative area of WTe₂. A distortion is clearly visible, as already reported in literature [S1, S2]. To assess if the observed distortion is confined at the surface, High Resolution Transmission Electron Microscopy was performed on freshly cleaved crystals at 10.5 K. Fig. S2 is a representative Selected Area Electron Diffraction (SAED) taken on a WTe₂ in the [011] zone. Diffraction spots are labeled in the SAED and compatible with those expected for the orthorhombic WTe₂ structure in the [011] zone axis. No signs of sublattices or structural distortions in the bulk of the crystal can be revealed by SAED investigation, confirming previous findings [S3].

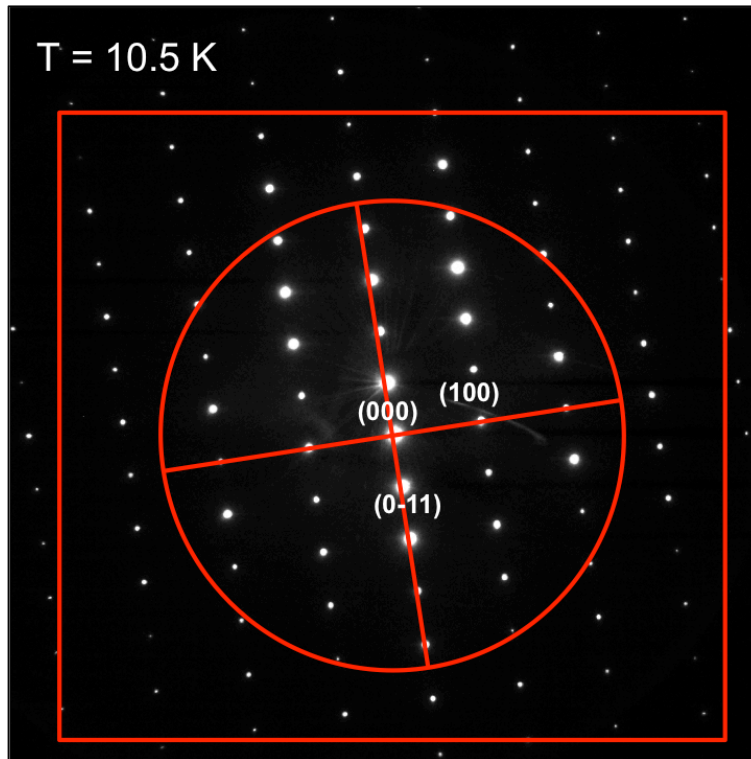


Figure S2: High Resolution Transmission Electron Microscopy of a freshly cleaved WTe_2 crystal.

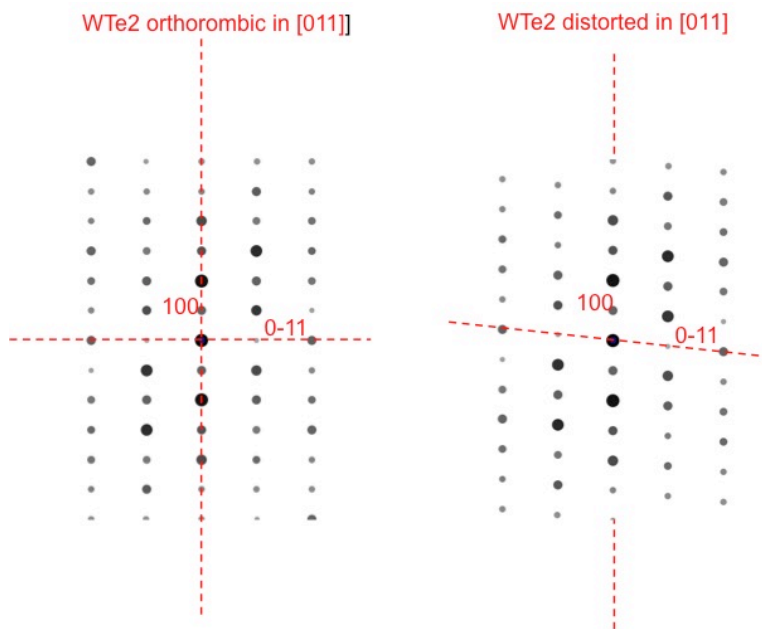


Figure S3: Simulation of non distorted (left) and distorted (right) diffractograms for orthorhombic WTe_2 . These results suggest that the observed distortion is confined at the surface region, and that the perturbation induced by the distortion does not give a detectable contribution to electron diffraction in the volume. To further confirm this observation, the difference between

diffractograms with and without a distortion have been simulated [S4]. Results are shown in Fig. S3, where the orthorhombic (left) and 6 degrees distorted (right) simulations are presented: the experimental SAED clearly agrees with the orthorhombic one.

Having ascertained that the distortion is confined at the surface, a further issue is to evaluate if the electronic band structure of the first layer(s) is affected and/or modified, thus possibly influencing the interpretation of the ARPES results. Fig. S4 presents band structure calculations with and without the observed surface distortion, calculated for one monolayer (i.e. in the case of the maximum effect possible), and taking into account the relaxation of neighboring atoms.

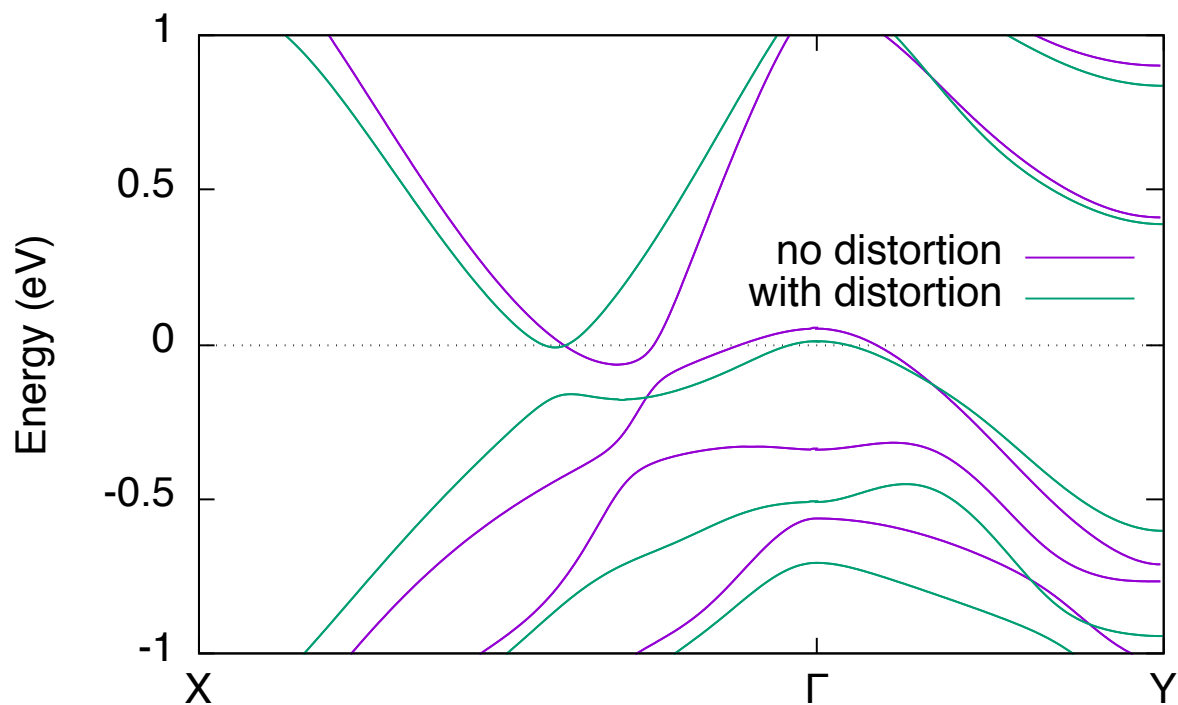


Figure S4: Band structure calculation of a monolayer of WTe₂ with and without the observed structure distortion of 6 degrees at the surface.

The distortion does not significantly modify the overall band structure and, more importantly, the hole-electron compensation is maintained. As for the broken symmetry and possible induced spin-polarization, the produced splitting is of the order of a few meV (< 5 meV) and localized only onto a single monolayer, thus not visible within our experimental resolution.

2. Inequivalent tellurium atoms at the surface.

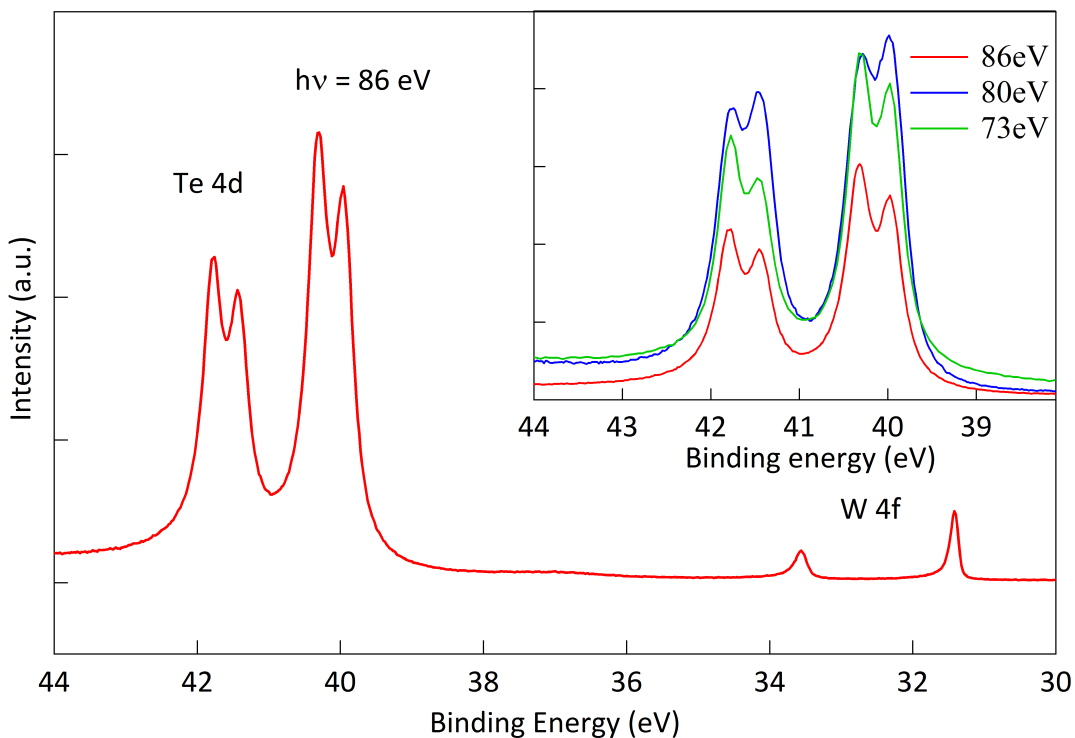


Figure S5: Te 4d and W 4f core level spectra of WTe_2 single crystal, measured at $h\nu=86$ eV (main panel), while W 4f level are single line peaks, a clear splitting is observed in the Te 4d. In the inset, intensity evolution of the Te 4d core level peak vs. photon energy; the ratio of the split peaks, in each spin orbit partner, changes vs. photon energy as due to photoelectron diffraction effects, thus indicating the presence of two inequivalent Te atoms. The spectra have been measured at temperatures below 77 K.

The observation of two inequivalent sites for Te in the STM characterization of the surface is confirmed by the core level photoemission results in Fig. S5, where Te 4d and W 4f shallow core levels are shown. Unlike the W 4f core level lines, each spin orbit partner of Te 4d is split into two components. The relative intensity of the peaks changes vs. photon energy. Because the photon energy range is too narrow to allow for cross section effects, this type of variation is the signature of photoelectron diffraction, as already observed in core level of topological insulators [S5], and confirming the existence of structurally and chemically inequivalent Te atoms in the Te-W-Te unit at the surface. This inequivalence is further confirmed by our ab-initio-calculated relaxed atomic positions to be present in the bulk and not only on the surface

layer. These findings are also consistent with structural data reported in Ref. [S6], showing two different W-Te bond lengths (2.71 and 2.81 Å) within each WTe₂ plane.

3. k_z dispersion

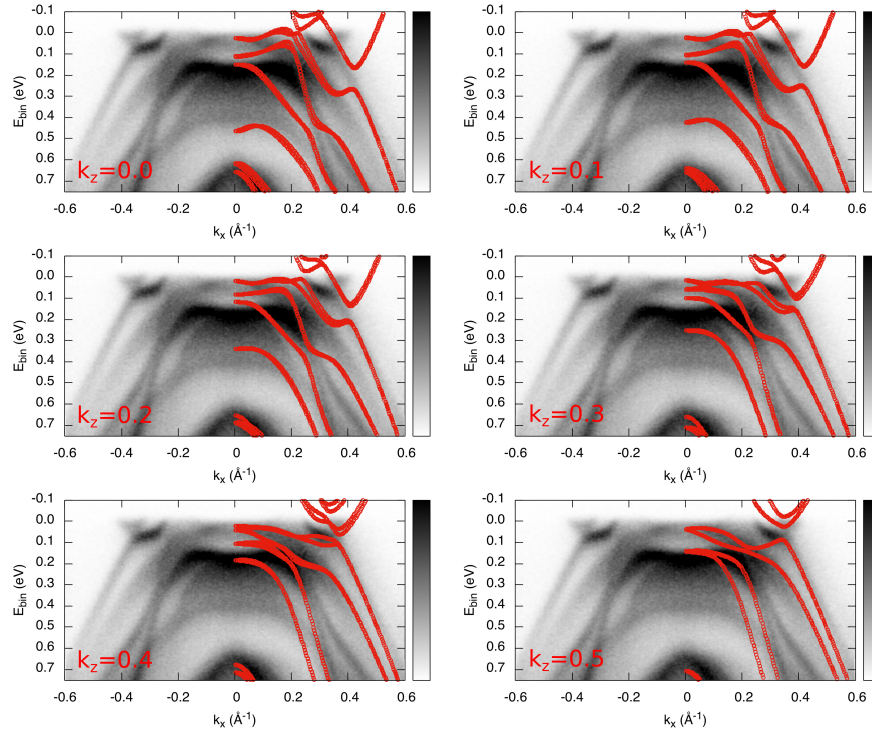


Figure S6: Theoretical DFT bandstructures for bulk WTe₂ along the line k_x for different out-of-plane k_z momenta overlaid to ARPES spectra. Values reported in the left bottom angle of the panels are in units of $2\pi/c$, and spin-orbit coupling has been taken into account.

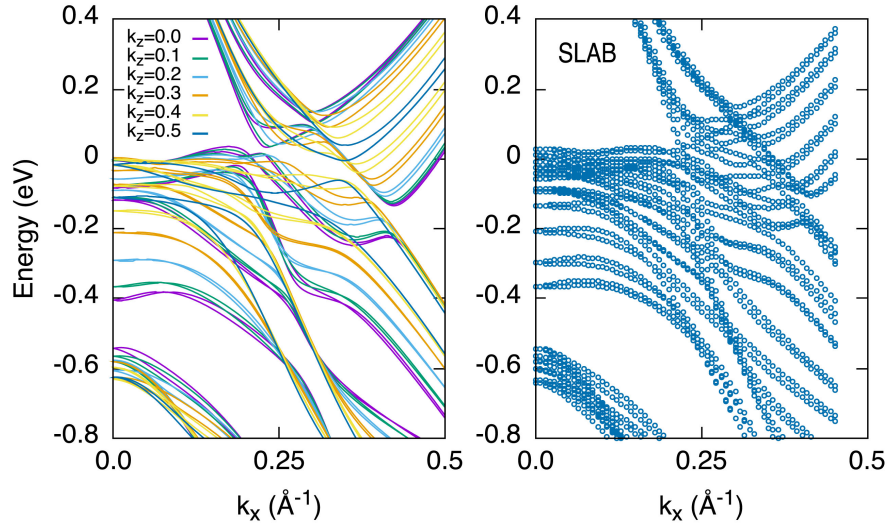


Figure S7: Left panel: Theoretical DFT bandstructures for bulk WTe2 along the line k_x for different out-of-plane k_z momenta. Values reported in the figure's caption are in units of $2\pi/c$, and spin-orbit coupling has been taken into account. Right panel: DFT bandstructure for a 6-layer-thick slab.

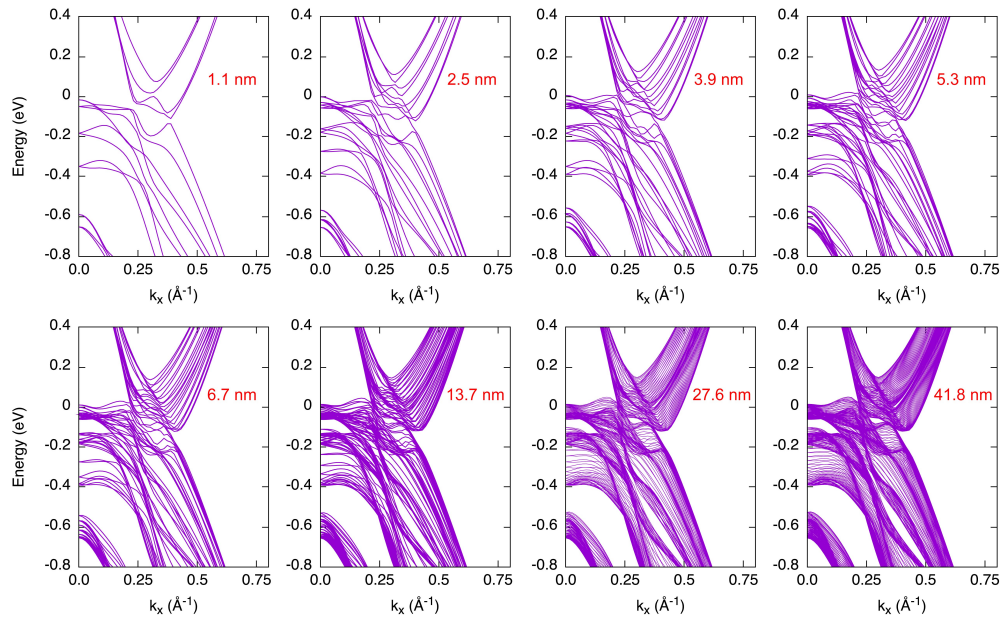


Figure S8: Ab-initio tight-binding model bandstructures for WTe2 film thicknesses ranging from 1.1 nm (2 WTe2 layers) to 41.8 nm (60 WTe2 layers) along the k_x reciprocal direction.

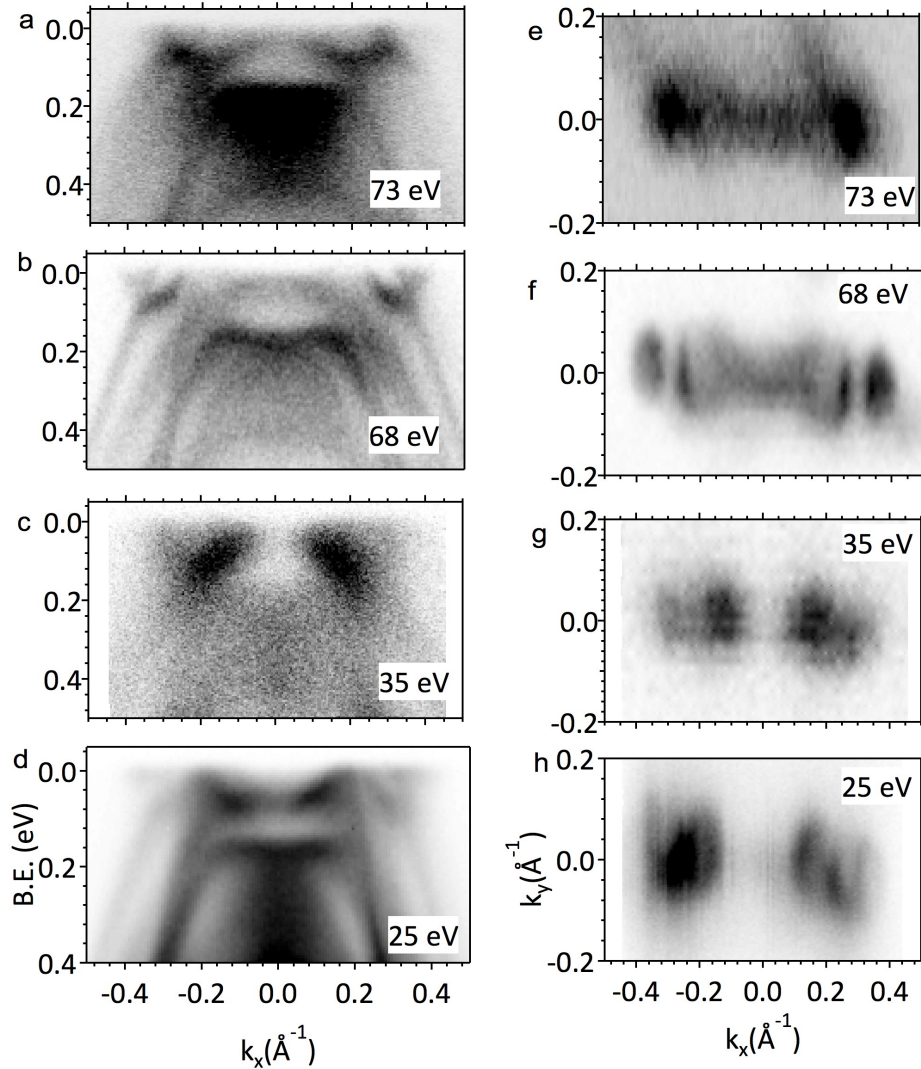


Figure S9: **Photon energy dependence of band structure.** The electronic band structure and Fermi surface are measured by ARPES at various photon energies. Panel a)–d) show the band structure along $\Gamma - X$ measured at photon energy 73, 68, 35, and 25 eV respectively, while panel e)–h) show the respective Fermi surface cuts. A clear photon energy dependence of band structure is observed. However, the overall size of Fermi surface area, and position of electron and hole pockets remain the same for all the energy values used in our experiment. A detailed photon energy dependence study has been done by Pletikosić et al. [S7], where they report a detailed k_z dependence.

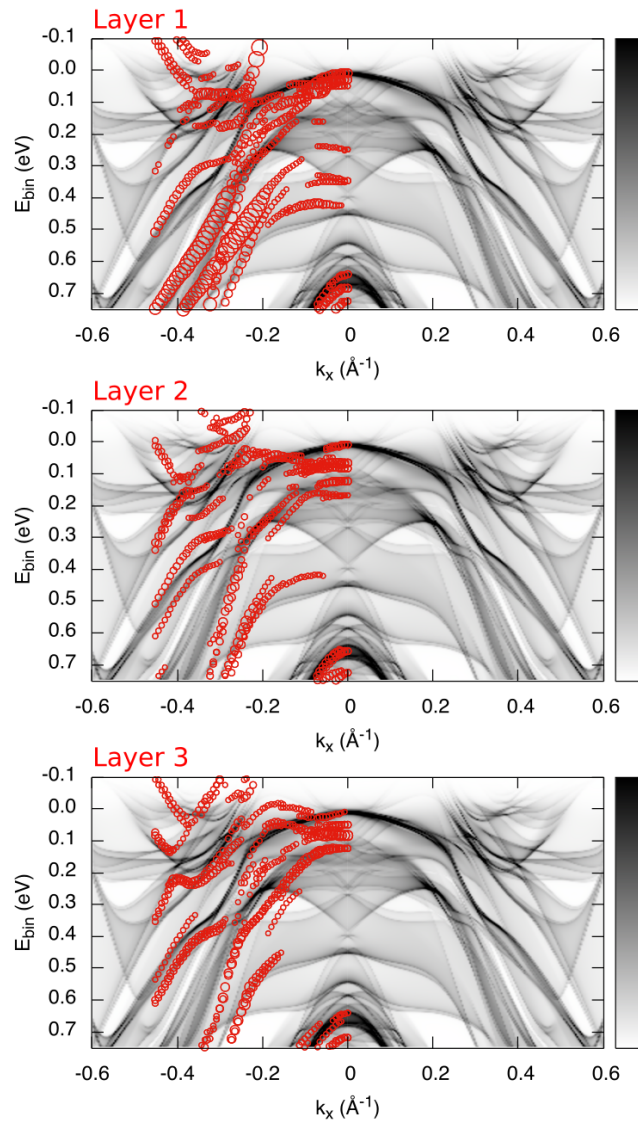


Figure S10: Theoretical surface spectral function (Fig. 2f in the main text) overlaid with layered resolved 6-layers-thick slab calculations (Fig. 2c-e).

- S1. A. Crossley, S. Myhra, C.J. Sofield: STM analysis of WTe₂ surfaces — correlation with crystal and electronic structures - *Surface Science*, 39-45 (1994)
- S2. S.W. Hlaa, V. Marinković, A. Prodana, I. Muševića: STM/AFM investigations of β -MoTe₂, α -MoTe₂ and WTe₂ - *Surface Science* **352-354**, 105-111 (1996)
- S3. Ali M. N., Xiong J. et al. Large, non-saturating magnetoresistance in WTe₂, *Nature* **514**, 205 -208 (2014).
- S4. P. Stadelmann (2006) JEMS Electron Microscopy Software, JAVA version 4.3030U2015, http://www.jems-saas.ch/home/jemsv4_3030u2015.htm];

- S5. Kuroda K., Ye. M et al. Experimental verification of the surface termination in the topological insulator TlBiSe₂ using core-level photoelectron spectroscopy and scanning tunneling microscopy, Phys. Rev. B **88**, 245308 (2013)
- S6. Mar A., Jovic S., Ibers A, Metal-metal vs tellurium-tellurium bonding in WTe₂ and its ternary variants TaIrTe₄ and NbIrTe₄, J. Am. Chem. Soc. **114**, 8963 (1992)
- S7. Pletikosić I., Ali M. N., Fedorov, A. V. Cava R. J., Valla T., Electronic Structure Basis for the Extraordinary Magnetoresistance in WTe₂, Phys. Rev. Lett. **113**, 216601 (2014)